On planar (110) channeling of 855 MeV electrons in a boron-doped diamond undulator

H. Backe[a,*], W. Lauth[a], P. Klag[a] and Thu Nhi Tran Caliste[b]

[a]Institute for Nuclear Physics of Johannes Gutenberg-University, Johann-Joachim-Becher-Weg 45, Mainz, D-55128, Germany,
[b]European Synchrotron Radiation Facility, 71 Avenue des Martyrs, Grenoble, F-38000, France,

ARTICLE INFO

Keywords:
Crystalline undulator
Channeling of electrons
Computer simulation calculations

ABSTRACT

A 4-period diamond undulator with a thickness of 20 μm was produced with the method of Chemical Vapour Deposition (CVC), applying boron doping, on a straight diamond crystal with an effective thickness of 165.5 μm. A planar (110) channeling experiment, performed with the high quality 855 MeV electron beam of the Mainz Microtron MAMI accelerator facility, failed to observe the expected undulator peak. Simulation calculations which are based on the continuum potential picture revealed unexpected results for radiation spectra at the chosen observation direction. They suggest, in addition, that at an optimized observation angle, for which the undulator peak is the strongest, the channeling radiation from the rather thick backing crystal can be significantly suppressed. A byproduct of this case study was the experimental observation that beam deflection can be achieved even with a flat 50 μm thick diamond crystal.

1. Introduction

There exists a long-lasting considerable interest in the channeling process of ultra-relativistic electrons and positrons at planes of a single crystal. Of particular interest is the emission of undulator-like radiation in periodical bent crystals aiming in the construction of compact radiation sources in the MeV range and beyond, see e.g. Korol et al. [1]. However, it is an experimental challenge to produce crystalline undulators with period lengthes in the order of a few μm range which are favourable at accelerator facilities delivering electron beams below an energy of about a GeV. Of potential interest are undulators based on diamond, because of its radiation hardness, which can be produced by Chemical Vapour Deposition (CVC) with periodically varying concentration of boron. The effect is based on the dependence of the lattice constant as function of the boron density resulting in oscillating (110) planes, see Fig. 1. In contrast to Ge-doped silicon undulators, the undulator structure cannot be separated from a host diamond crystal, meaning that in an experiment one is always faced with radiation from the backing.

In this paper we describe experiments with an 4-period diamond undulator with a thickness of 20 μm at planar (110) channeling, performed with the high quality 855 MeV electron beam of the Mainz Microtron MAMI accelerator facility. The undulator chip was produced with the method of Chemical Vapour Deposition (CVC), applying boron doping, on a straight diamond crystal with an effective thickness of 165.5 μm, the effective thickness is the slab thickness multiplied by $\sqrt{2}$. During the course of the experiment it became apparent that for an on line optimization a computer code would be desirable which delivers useful results with moderate CPU times and runs, very important, on a personal computer. In contrast to very precise results obtained with the rather sophisticated MBN explorer code by Pavlov et al. [2], also for a diamond undulator, for our code a compromise must be found between efficiency and accuracy. The paper addresses these issues.

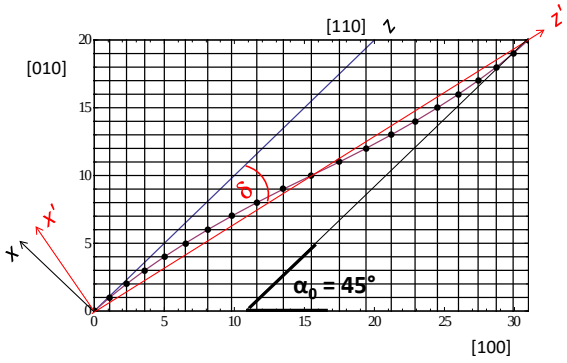

Figure 1: One period of the undulator crystal. The z direction coincides with the [110] direction of the host crystal, which is not shown but can be imagined as continuation to the right hand border, and makes an angle $\alpha_0 = 45°$ with respect to the [100] direction. At observation along the z' axis which makes an angle δ with respect to the [110] direction an undulator structure is clearly recognizable. Planes are formed perpendicular to the shown plane of drawing, the y - direction.

The paper is organized as follows. In section 2 the design parameters of the undulator are described, and in section 3 the experimental setup at MAMI including the measurements. Since the expected undulator peak was not observed, simulation calculations were performed in order to contribute to an explanation of this result. The calculations are based on the continuum potential picture introduced originally by Lindhard [3]. The formalism described in section 4 is based on [4, 5], extended to undulator crystals, and to the calculation of radiation spectra. For the latter a

backe@uni-mainz.de (H. Backe)
ORCID(s):

formula of J.D. Jackson's textbook "Classical Electrodynamics" was used which involves explicitly the acceleration of the particle. It is also the basis of our approach to develop an efficient computer code as an aid for an on-line optimization during the course of an experiment. In section 5 results are presented and discussed. Some details on the basics of the simulation calculation for the radiation spectra are described in an appendix. The paper includes also experiments and a discussion in section 6 on the possibility to deflect the electron beam with a straight crystal at oblique incidence.

2. The diamond undulator

A boron-doped undulator has been produced by Chemical Vapour Deposition (CVC) with the following design parameters: period length in [100] direction $\lambda_U = 5/\sqrt{2}\ \mu$m, number of periods $N_U = 4$, and a thickness of the chip, the host crystal, of 117 μm. The design profile of the boron doping in [100] direction is of triangular shape with the minimum and maximum boron content $n_{B,min} = 6 \cdot 10^{20}$/cm³ and $n_{B,max} = 24 \cdot 10^{20}$/cm³, corresponding to a concentration of $c_{min} = 0.00340$ and $c_{max} = 0.0136$, respectively. Analytically, the boron content reads as function of the z coordinate for the first half period $c(z) = c_{min} + 2(c_{max} - c_{min}) \cdot z/\lambda_U$, $0 \le z \le \lambda_U/2$. The continuation to $\lambda_U/2 < z \le \lambda_U$ can be obtained by symmetry considerations.

Following the formalism described for $Si_{1-c}Ge_c$ in [6, Appendix A], the lattice constant has been parameterized as

$$a_{\perp CB} = a_C + a_1\, c + a_2\, c^2 + \frac{2C_{12}}{C_{11}}\left(a_1\, c + a_2\, c^2\right). \quad (1)$$

with the elastic constants

$$C_{11} = C_{11}^{(0)} + C_{11}^{(1)}\, c \quad (2)$$

$$C_{12} = C_{12}^{(0)} + C_{12}^{(1)}\, c. \quad (3)$$

and the numerical values $C_{11}^{(0)} = 1.0764 \cdot 10^{12}$ Nm^{-2}, $C_{11}^{(1)} = 0$, $C_{12}^{(0)} = 0.125 \cdot 10^{12}$ Nm^{-2}, and $C_{12}^{(1)}$=0 [7]. The quantity $a_C = 0.35668$ nm is the lattice constant of diamond [7], and the quantities $a_1 = 0.0274$ nm, $a_2 = 0$ were derived from the "atomic volume interpolation" curve depicted in Fig. 2.

With the abbreviation $k = (1 + 2C_{12}/C_{11}) \cdot a_1/a_C = 0.09474$ and $\delta a_{\perp CB}/a_{\perp CB}(z) = k \cdot c(z)$ one obtains the differential equation $dx/dz = -k \cdot c(z)$ for the bent (110) channel. Notice that beside the boundary condition $x(z \to 0) = 0$ also $dx/dz(z \to 0) = 0$ must be fulfilled. The solution is schematically shown in Fig. 1. It defines the (x', z') coordinate system, in red color, with the z' axis through the turning point of the derivative, rotated clock wise by an angle δ with respect to the nominal [110] direction of the undoped diamond crystal. Numerically δ = -0.484 mrad is obtained.

The radius of curvature is approximately given by $R_{bent} = \left(d^2x/dz^2(z)\right)^{-1}$ which turns out to be a constant for half a period. This is a consequence of the assumption of a linear doping profile, with $a_2 = 0$, and $C_{11}^{(1)} = C_{12}^{(1)} = 0$, which considerably simplifies the calculation to be described in the following. Numerically one obtains $R_{bent} = \pm\ 2.584$ mm. Another consequence of these special assumptions is that the acceleration is of square waveform, see Fig. 7 (a), rather than of a sinusoidal one, as commonly assumed in calculations of radiation emission spectra.

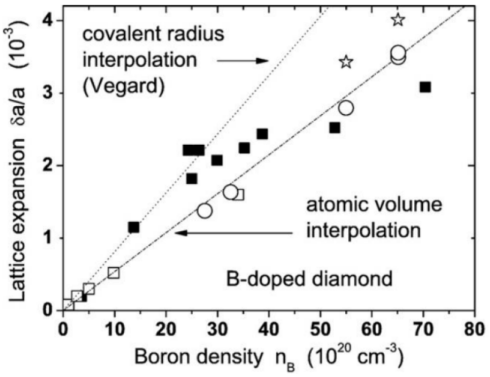

Figure 2: Lattice expansion as function of the boron density.

3. Experimental

The experimental setup at the Mainz Microtron MAMI is shown at Fig. 3. The electron beam is focused onto the diamond target in the target chamber with goniometer and thereafter deflected by a dipole magnet into the second beam profile chamber in which the scattered beam can be observed with a LYSO fluorescence screen. The target can be rotated in all 3 spatial directions with an accuracy of 35 μrad. The target is aligned using the signal of the ionization chamber that registers the scattered electrons. The orientation of a plane parallel to the electron beam increases the scattering probability and, in turn, the signal of the ionization chambers. This method allows rapid orientation of a crystal plane. The radiation in the forward direction is detected with a 10 inch NaI crystal, positioned at a distance of about 8.5 m from the target. A movable cylindrical tungsten aperture with a bore of 4 mm diameter in front of the detector defines the observation direction. The alignment of the aperture was done by maximizing the detected bremsstrahlung from an aluminum foil.

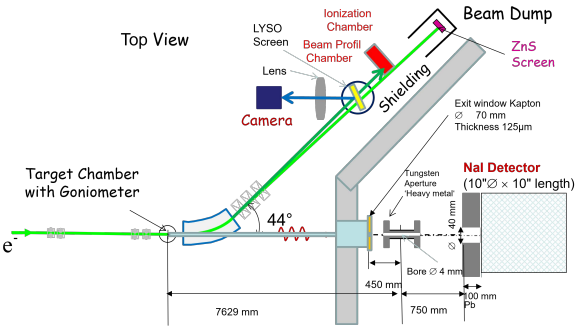

Figure 3: Experimental setup at MAMI. Radiation is observed in collinear geometry with the electron beam.

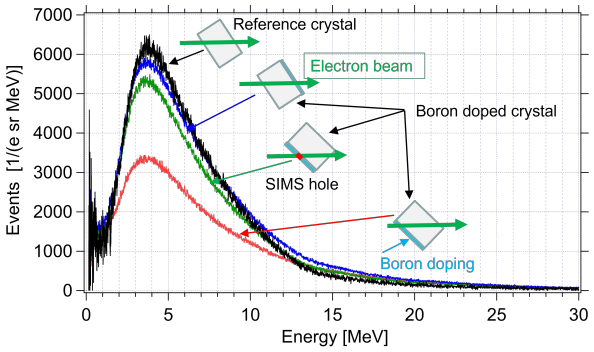

Figure 4: Experimental radiation spectra at (110) channeling for the boron-doped diamond crystal ('Boron doped crystal'), and the reference crystal with an effective thickness of 101 $\sqrt{2}$ μm = 143 μm ('Reference crystal'). The former spectra were taken at three different geometries: (i) beam enters first the boron doped layer and thereafter the backing (red), (ii) beam enters first the backing and at the end the boron doped layer (blue), and (iii) beam enters the SIMS hole, at which the boron doped layer was removed (green). Spectra of random orientation of the crystal were subtracted. Spectra were taken at a typical beam current of 10 fA.

Fig. 4 depicts relevant spectra taken with the sodium iodide detector at collinear alignment of beam and detector aperture. The boron doped crystal and a 101 μm thick undoped reference crystal with the same surface orientation were moved into the center of the goniometer. The boron doped layer was removed at a specific position with an area of 0.8 mm x 0.8 mm for a measurement of the doping profile with the aid of the secondary ion mass spectroscopy method (SIMS). Spectra were also taken at the position of this SIMS hole and, in addition, with the crystal rotated on an axis perpendicular to the plane of drawing by 180°. If the electron beam first enters the boron-doped layer and thereafter the straight backing crystal, the channeling radiation is suppressed (red spectrum). The broad peak structure at about 4 MeV is due to channeling radiation.

No peak was found near the expected energy of 1.15 MeV. There are, of course, a number of reasons for this negative result, including that with the Chemical Vapour Deposition (CVC) procedure the envisaged structure on the 117 µm backing crystal was not prepared. In this paper we investigate additional possible reasons by means of simulation calculations assuming the ideal undulator structure as described in section 2.

4. Description of the simulation model

The starting point for the calculation of the radiation spectra is the following formula of J.D. Jackson's textbook "Classical Electrodynamics" [8, Eq. (14.65)]:

$$\frac{d^2I}{d\omega d\Omega} = \frac{e^2}{4\pi^2 c}\left|\int_{-\infty}^{\infty} \frac{\hat{n}\times[(\hat{n}-\vec{\beta})\times\dot{\vec{\beta}}]}{\left(1-\vec{\beta}\cdot\hat{n}\right)^2} e^{i\omega\left(t-\hat{n}\cdot\vec{r}(t)/c\right)}\,dt\right|^2 \quad (4)$$

with d^2I the radiated energy with radial frequency ω into the interval $d\omega$ and solid angle element $d\Omega$, $\hat{n}$ the observation direction, $\vec{\beta} = \vec{v}(t)/c$ with $\vec{v}(t)$ the particle velocity, $\vec{r}(t)$ the electron trajectory in the laboratory system, and $e^2 = \hbar c\alpha$ with α the fine structure constant and c the speed of light. For the approximate evaluation of this equation various assumptions have been made. It is assumed that (i) the electron is highly relativistic with a Lorentz factor $\gamma = 1/\sqrt{1-\beta^2} \gtrapprox 1000$, that (ii) the deviation of the trajectory from the initial beam direction is very small, in the order of some tenfolds of Angstroms, that (iii) the undulator period λ_U is very short, in the order of a couple of μm, that (iv) the thickness of the emitting layer is less than about 200 μm, that (v) the distance between undulator and observation point is very large, in the order of 5-10 m, that (vi) for the observation angle with respect to the beam direction $\theta \ll 1$ holds, and (vii) that the emitted photon energy is small, i.e. $\hbar\omega \ll \gamma m_e c^2$, with m_e the rest mass of the electron.

Radiation emission occurs if the beam particle experiences acceleration caused by an external field, in our case it is of electrostatic origin. There are two types of acceleration which are the transverse and the longitudinal one. Let us first consider the transverse acceleration for which Eq. (4) can be cast into the form (for details see appendix)

$$\frac{d^2N\hbar\omega}{d\hbar\omega d\Omega} = \frac{\alpha}{4\pi^2}\left|\int_0^{\zeta_0} 2\gamma^2 \frac{[-1+\gamma^2(\theta-\vartheta(\zeta^{-1}))^2]}{[1+\gamma^2(\theta-\vartheta(\zeta^{-1}))^2]^2}\cdot\vartheta'(\zeta^{-1}) \times \frac{1}{[1+\gamma^2(\theta-\vartheta(\zeta^{-1}))^2]}\; e^{i\,\overline{\omega}\,\zeta} d\zeta\right|^2. \quad (5)$$

Here are

$$\overline{\omega} = \frac{\hbar\omega}{2\gamma^2\hbar c} \text{ and } \zeta = z + \int_0^z \gamma^2(\theta-\vartheta(z'))^2 dz' \quad (6)$$

with $\vartheta(z)$ the projected angle onto the x-z plane of the particle trajectory. It is the derivative of the electron trajectory as function of the z coordinate which coincides with the beam direction with its origin at the entrance of the crystal. The quantity $\vartheta'(z)$ is the derivative of $\vartheta(z)$. The expression in the first row of Eq. (5) corresponds to the acceleration expression in Eq. (4), that one in the second row to $\left(t-\hat{n}\cdot\vec{r}(t)/c\right)$ in the exponential which results in Eq. (6). The angle θ signifies the projected observation direction. The derivative $d\zeta/dz$ allows substitution of the integration variable after which the integral is cast into the standard form of a Fourier representation. The consequence of the substitution is that the inverse function of Eq. (6) $\zeta^{-1}(z)$ appears in Eq. (5). The upper integral limit is $\zeta_0 = \zeta(z_0)$, with z_0 the length of the undulator including the backing.

The longitudinal acceleration originates from the energetic coupling between the transverse and longitudinal degrees of freedom, resulting in the well known 'figure eight' motion. For the small angles with respect to the beam direction which are in the order of a few mrad the transverse energy $(pv/2)\,\vartheta^2$, with pv associated to the momentum of the particle, is in the order of less than about 10 keV

which is very small in comparison with the beam energy of 855 MeV. We mention that a longitudinal acceleration would result in a formula like Eq. (5), in which the term $[-1+\gamma^2(\theta-\vartheta(\zeta^{-1}))^2]$ in the nominator is replaced by the observation angle θ. Since the resulting additional summand from the longitudinal acceleration is of higher order type in comparison with the lateral acceleration, it can safely be neglected.

The differential photon number spectrum per relative band width $d\hbar\omega/\hbar\omega$ and solid angle element $d\Omega$ is the power spectral density

$$\frac{d^2N}{d\hbar\omega/\hbar\omega\, d\Omega} = \frac{\alpha}{4\pi^2}\left|\int_0^{\zeta_0}\overline{\vartheta'(\zeta^{-1})}e^{i\,\overline{\omega}\,\zeta}d\zeta\right|^2 = \\ = \frac{\alpha}{4\pi^2}\left(\Delta\zeta\; S_{PSD}(\overline{\vartheta'_{dig}(\zeta^{-1})},\overline{\omega}\Delta\zeta)\;\zeta_0\right). \quad (7)$$

The integral is taken over the complete thickness ζ_0 of the matter sheet which may contain an undulator and, in addition, a plane section, ensuring a coherent superposition of both parts. The quantity S_{PSD} denotes the expression PowerSpectralDensity[data, ω] of Mathematica 13, a very efficient routine, and $\Delta\zeta$ the digitizing interval of the derivative $\overline{\vartheta'(\zeta^{-1})}$ which represents the complete expression in front of the exponential in Eq. (5) under the integral. The quantity $\overline{\vartheta'_{dig}(\zeta^{-1})}$ denotes the digitized version of the acceleration function $\overline{\vartheta'(\zeta^{-1})}$. This quantity can be derived from the simulated $\vartheta(z)$ from which the undulator spectrum and also the channeling radiation spectra can be calculated, in which effects of random scattering at atoms and electrons are included.

A remark seems to be appropriate why [8, Eq. (14.65)] of Jackson's textbook has been used rather than the partially integrated simpler [8, Eq. (14.67)]. The reason is that phase factors occur at the analysis of the latter, resulting from non vanishing entrance and exit angles, which prevent a Fourier representation.

5. Results and Discussion

The potential in which the particle moves has been calculated as described for a plane crystal in [4, see Fig. 2(a)] to which the centrifugal potential $U_c(x) = \pm\gamma m_e c^2\beta^2/R_{bent}\cdot x$ was added. The potentials are shown in Fig. 5. As the particle moves through the undulator crystal, the potential flips at depths $z = n\lambda/2$, with n an integer, between both potential states. In the formalism described in [4], the scattering angle $\vartheta(z) = dx/dz(z)$ as function of the depth z has been calculated in a digitized form, taking into account collisions between the particle and atoms and electrons. This is just the quantity which enters in Eqs. (5) and (6) as $\vartheta(\zeta^{-1})$ and $\vartheta'(\zeta^{-1})$ for the calculation of the radiation spectra.

5.1. Angular Distributions

In the following it is assumed that a narrow electron beam with an angular divergence $\sigma_x = 0.0127$ mrad impinges the undulator crystal with the projected angle $\psi = 0$ the electron beam makes with the (110) plane. For the latter it is assumed that the crystal was aligned into the beam direction, i.e., in Fig. 1 at $\alpha_0 = 45°$. The scattering distribution of the electrons after passage of the undulator at $z = 20$ μm is shown in Fig. 6 (a). The undulator effects a dramatic broadening and also a clockwise shift of the initial electron beam distribution. With this angular distribution the electron enters the straight undoped backing crystal. As demonstrated in part (b) of the figure, the angular distribution broadens further and apparently suffers an additional shift. A possible reason for the latter will be treated in more detail in chapter 6 below. Quantitatively, the angular distribution is rotated clockwise by about 0.4 mrad with a long extension up to -1 mrad. These facts may complicate a proper alignment of the undulator crystal into the nominal direction. It might well be that with the procedure described above the alignment results in an oblique incidence of the beam into the undulator crystal.

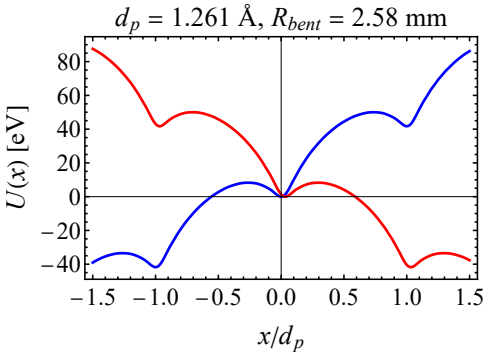

Figure 5: Potentials for deformed (110) planes in diamond.The blue curve holds for the first half period $0 \le z \le \lambda_U/2$ of the undulator, the red one for the second one with $\lambda_U/2 < z \le \lambda_U$. The interplanar distance is $d_p = \sqrt{2}a_C/4 = 0.1261$ nm.

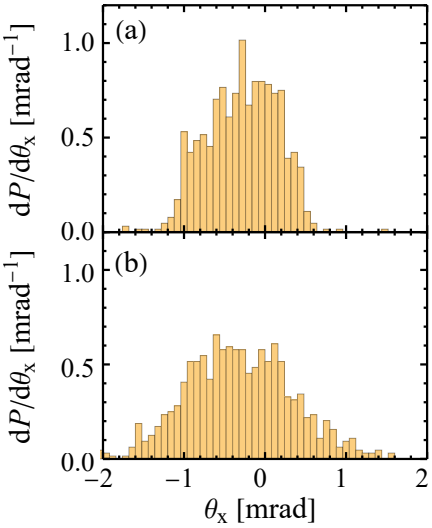

Figure 6: Simulated scatter distributions of the electron beam, (a) only for the 4-period undulator of 20 μm thickness, (b) undulator plus 165.5 μm thick straight backing part.

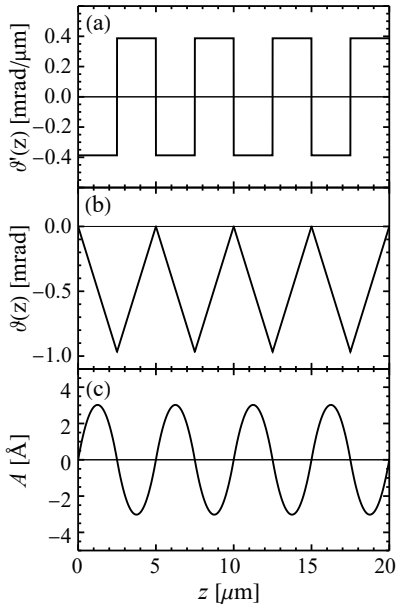

Figure 7: Model trajectories for (a) acceleration $\vartheta'(z)$, (b) slope of the trajectory with the initial condition $\vartheta(0) = 0$, and (c) amplitude $A(z)$ with $A(0) = 0$ and $\vartheta(0) = -\delta = 0.484$ mrad, i.e. in the primed coordinate system of Fig. 1.

5.2. Radiation spectra

Assuming that the undulator crystal was aligned properly in such a manner that the electron beam coincides with the $\alpha_0 = 45°$ direction, see Fig. 1, there exist two favourable observation directions in θ. One is the forward direction $\theta = 0$ in which the radiation detector is on-axis with the electron beam direction, i.e., in Fig. 1 with the z axis. The other one would be the undulator radiation direction in which the radiation detector is rotated counter clockwise by the angle $\theta = \delta =$ -0.484 mrad. To make the effects clear, radiation spectra were created on the basis of the formalism described in section 4 separately for the 4-period undulator crystal alone, and for the undulator chip consisting of both, undulator part and the straight backing crystal.

5.2.1. Model calculations

In a first step we construct an ideal model trajectory on the basis of the square wave acceleration profile neglecting any interaction with atoms and electrons. This means, the particle sticks in the potential minimum without experiencing an excitation. In Fig. 7 the acceleration, the derivative and the amplitude are shown, the latter with respect to the rotated primed coordinate system in Fig. 1. The radiation spectrum according to Eq. (5) can explicitly be calculated since all the quantities under the integral can be extracted from the acceleration profile $\vartheta'(z)$. Fig. 8 depicts calculated photon number spectra at the two mentioned observation directions θ. The black spectrum, taken in undulator direction, i.e. the z' direction in Fig. (1), reveals a significant peak. The

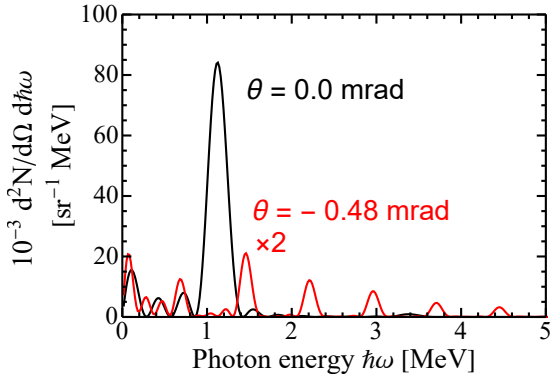

Figure 8: Calculated photon number spectra for the 4-period undulator without radiation from the straight section of the undulator chip. Spectra in black color for observation in undulator radiation direction, i.e., in the z' direction of Fig. 1, in red color observation in forward direction, i.e., in the z direction of Fig. 1, enlarged by a factor of two.

peak energy can be calculated with the well known relation

$$\hbar\omega = k\frac{4\pi\gamma^2\hbar c}{\lambda_U\left(1 + K^2/2 + (\theta\gamma)^2\right)}. \quad (8)$$

In lowest order $k = 1$, observation in forward direction $\theta = 0$, amplitude $A = 0.302$ nm, period length $\lambda_U = 5.0$ μm, undulator parameter $K = \gamma \cdot A \cdot 2\pi/\lambda_U = 0.656$, for the peak energy $\hbar\omega = 1.14$ MeV is obtained in accordance with the energy of the simulated peak. The additional low energy structures are interpreted as interferences since Eq. (5) is

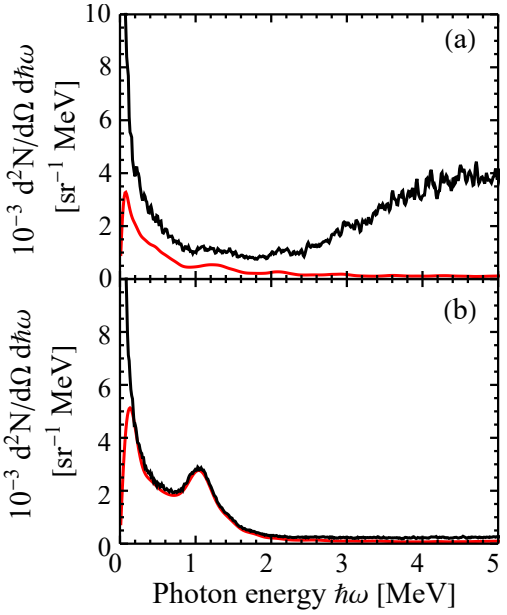

Figure 9: Photon number spectra for the 4-period undulator plus backing at observation in forward direction $\theta = 0$ mrad (a), i.e., in the z direction of Fig. 1, and $\theta = \delta = -0.484$ mrad (b), i.e., in the z' direction of Fig. 1. For comparison the undulator contribution alone is shown in red color. Mean of 400 sample trajectories.

a phase integral. Such interferences are well known, and are described in literature for magnetic undulators with a $\left(\sin(x-x_0)/(x-x_0)\right)^2$ structure. This is an approximation for many periods, however, we are dealing with only 4 periods and such a simple formula does not hold anymore.

At observation in forward direction $\theta = 0$ one naively expects from the common undulator theory a Doppler-shifted lower energy peak at 0.743 MeV with somewhat reduced intensity, and probably a second order one. However, the calculated spectrum revealed to our surprise a completely different spectrum, see the spectrum in red color in Fig. 8. However, at closer inspection the first and second order peaks can clearly be recognized, including a number of higher order peaks. Indeed, such a fragmented spectrum is expected also from the magnetic undulator theory at off axis observation and large undulator parameters K, see e.g. [9, Fig.2.3]. It is worth noting that Eq. (5) represents all orders of the harmonics at once, i.e. it is not an expansion in terms of the harmonics.

Finally we mention that straight injection of the particle into the potential wall results in a lateral displacement of the beam. As a consequence, the crystal undulator radiation is emitted not in forward direction but sidewards at a certain observation angle θ, being the true reference direction. This fact should be taken into account not only at the stage of the design of an undulator structure but, in particular, in the course of the experiment.

5.2.2. Simulation calculations

In this subsection we describe full-fledged simulation calculations in the real potential taking into account interactions of the beam electron with atoms and bulk electrons. In Fig. 9 the results are shown. The lower part (b) shows spectra at observation in undulator direction, i.e. at $\theta = \delta = -0.484$ mrad. The undulator peak remains clearly visible, however, it is a factor of about 50 weaker. Notice, the scale has been enlarged by a factor of 10 in comparison with Fig. 8. The upper part (a) shows spectra at observation in forward direction $\theta = 0$. There seem to be indications of broad structures at position of the first and second harmonics, and perhaps also higher ones, see spectrum in red color.

At observation in undulator direction the channeling radiation from the rather thick backing of 165.5 μm is strongly suppressed. However, it must be mentioned that the calculations have been performed for ideal experimental conditions. In a real experiment the dimension of the detector aperture in the order of 0.5 mrad results in an increase of the channeling radiation background. In addition, the low energy noise may be larger, and also tails of the channeling radiation originating from the detector response function will deteriorate these predictions, not to mention that also the undulator may not be ideal, and that various assumption made for design of the undulator were not met.

Fig. 4 shows a significant difference between the spectrum which was taken if the beam enters first into the undulator crystal and thereafter into the flat backing crystal (red) and for the reversed orientation of the chip, i.e. first into the backing crystal and thereafter into the undulator (blue). Such an effect is expected from the broadening and shift of the scattering distribution originating from the undulator crystal as shown in Fig. 6 (a). This distribution is of significant difference as compared with the narrow beam distribution which enters the backing crystal in the reversed configuration. Simulation calculations for both cases are shown in Fig. 10. They reproduce quite well the intensity ratio. This fact suggests that there must exist at least for half a period an undulating structure as designed which deflects the beam. The simulated spectrum of a complete amorphous structure as shown in Fig. 10 (b) is at variance with the observation, see Fig. 4 (red spectrum), and can be excluded.

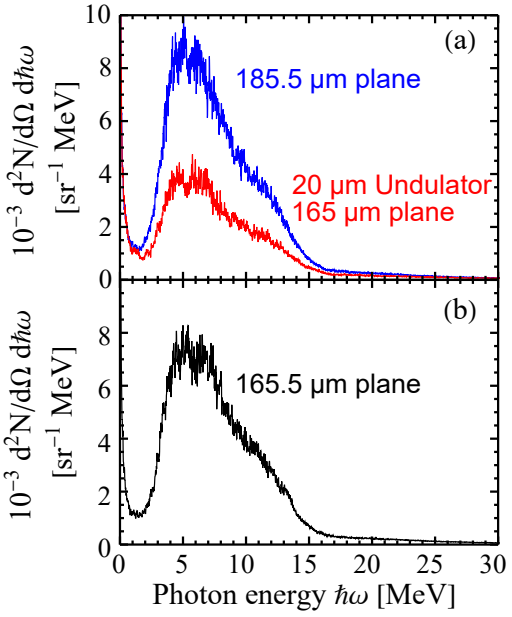

Figure 10: (a) Photon number spectra for an effective 185.5 μm thick plane crystal in (110) orientation at observation in forward direction at $\theta = 0$ mrad, i.e., in the z direction of Fig. 1 (blue), together with the spectrum for a 4-period 20 μm thick undulator crystal and a 165.5 μm thick plane backing crystal behind (red). (b) Spectrum of a 165.5 μm thick plane crystal with a broadened entrance distribution of the beam of $\sigma_x = 0.137$ mrad which simulates a 20 μm amorphous entrance layer. Mean of 400 sample trajectories.

We mention that the simulation calculations for the flat crystal, Fig. 10 (b) with a thickness of 165.5 μm, does not perfectly reproduce the measured channeling radiation distribution. The reason might be found in the simulation of the trajectory at the passage of the electron through the rather thick crystal. However, the absolute peak intensity is, with a larger intensity of about 20 %, quite close to the observation. In case that in the experiment the crystal was not perfectly aligned, the peak intensity would be reduced and, at the same time, the peak energy be shifted to lower energies, reducing the variance between experiment and observation.

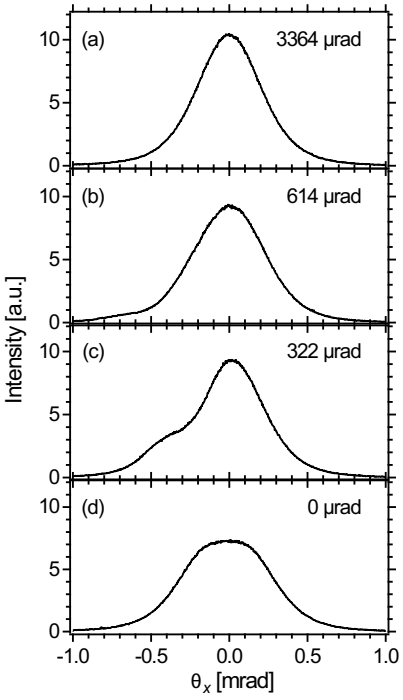

Figure 11: Experimental scatter distributions of an 855 MeV electron beam impinging on a 50 μm thick plane diamond crystal at projected tilt angles ψ as indicated in the sub pictures. In part (c) the deflectted distribution is clearly visible.

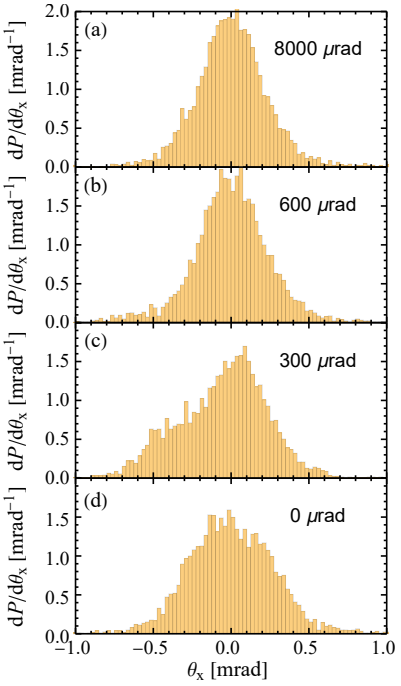

Figure 12: Simulated scatter distributions of an 855 MeV electron beam impinging on a 50 μm thick plane diamond crystal with projected tilt angles ψ as indicated in the sub pictures.

6. Beam deflection with a plane crystal

Downstream the target the beam profile can be observed with a fluorescence screen and a camera system as shown in Fig. 3. For a 50 μm thick diamond single crystal an asymmetric scattering distribution was observed at various incidence angles ψ between electron beam and the (110) plane. The phenomenon, depicted in Fig. 11, can be reproduced with our simulation calculations as shown in Fig. 12. It is interesting to note that at part (c) the side peak seems to be roughly correlated to the entrance tilt angles. This fact suggests that the beam deflection is connected with the channeling phenomenon. At 0.3 mrad the initial transverse energy amounts to 38 eV meaning that the electron moves in a sort of above barrier channeling over the (110) potential walls with a depth of 24 eV. At scattering close to the potential minimum, where the atomic density is largest, the electron may be captured and continues propagation in the channeling mode. In that case it may exit the crystal at about the entrance tilt angle. However, the exit distribution will be broadened depending on the transverse energy and the phase of the oscillation at exit. Once a channeled particle dechannels again, some memory effects that it was in between in the channeling mode may remain. This conjecture is in accordance with simulation calculations selecting only events which were temporarily channeling in a region about 25 μm from the exit, see Fig. 13.

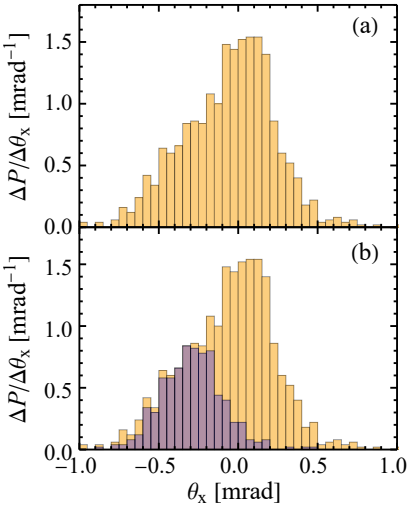

Figure 13: Decomposition of the scatter probability of the 50 μm thick plane diamond crystal at a tilt angle of 0.3 mrad. At (a) the simulated scatter distribution is shown, at (b) together with the contribution of particles which experienced temporarily channeling in the last 25 μm.

7. Conclusions

A boron-doped 4-period diamond undulator with a thickness of 20 μm, grown on a plane crystal with an effective thickness of 165.5 μm, was investigated experimentally at MAMI and with the aid of simulation calculations. The latter are based on an equation taken from Jackson's textbook

which explicitly contains the acceleration of the particle resulting in Eq. (5) which is assumed to be rather precise for the parameters of this investigation. Although the model assumptions on the boron-doping profile and in turn the acceleration profile are unrealistic, various possibilities for the unsuccessful search for a peak structure could be addressed in this case study. The simulation calculations revealed, as only one possible reason, that the observation direction in forward direction was not properly chosen. In a future experiment the detector must be rotated into the z' direction, see Fig. 1. The low undulator radiation intensity shown in Fig. 9 is a consequence of a too strong doping of the undulator part, resulting in low potential minima, see Fig. 5, and consequently strong de-channeling. The background from the straight section of the undulator chip has under ideal experimental conditions apparently only little impact on the observation of the undulator peak.

The peculiar result of the simulation calculation with observation in forward direction is a consequence of the fact that the undulator was not designed with a quarter period at entrance which would rotate the undulator in beam direction. Such design maintains also an angle δ between undulator and backing crystal, and the channeling radiation from the backing will also be suppressed. The design of such an undulator might be somewhat more complicated in comparison with that one described in this paper. Since the results of both geometries are the same, the simpler design should be preferred.

Deeper insight into the performance of an undulator, in particular for radiation production, may be gained with positrons. A 530 MeV beam is now available at MAMI which was constructed on the basis of Ref. [10].

The scattering distribution at tilted injection of the beam into a 50 μm thick plane crystal indicates that a partial beam deflection can be achieved even with the aid of a plane crystal. Simulation calculation suggest that the effect originates from rechanneling of the incident particle.

Acknowledgements

Fruitful discussions with A. V. Korol, and A. V. Solov'yov are gratefully acknowledged.

Declarations

This work has been financially supported by the European Innovation Council (EIC) Pathfinder TECHNO-CLS project 101046458.

Data availability statement

All data are freely available.

A. Derivation of equation (5)

In this appendix some details are presented how Eq. (5) comes about and which accuracy is expected in applying it. We repeat that the expression in the first row of Eq. (5) corresponds to the acceleration expression in Eq. (4), and that one in the second row to $\left(t-\hat{n}\cdot\vec{r}(t)/c\right)$ in the exponential which results in Eq. (6). The acceleration expression can be rewritten with the angular quantities defined below Eqs. (5) and (6) in the text for the x component as

$$\frac{\cos[\theta]\cdot\left(1-1/\gamma^2-\sqrt{1-1/\gamma^2}\cos[\theta-\vartheta]\right)}{\left(-1+\sqrt{1-1/\gamma^2}\cos[\theta-\vartheta]\right)^2}A_c. \quad (9)$$

A second order expansion of $\cos[\theta-\vartheta]$ and $\beta=\sqrt{1-1/\gamma^2}$ yields with the acceleration A_c, which is the prefactor of the vector $A_c\beta\left(\cos[\vartheta]\hat{e_x}-\sin[\vartheta]\hat{e_z}\right)$, and with the approximation $A_c\simeq\vartheta'$, the first row of Eq. (5). The expansion has for our parameters a relative accuracy of less than about 10^{-6}.

For the exponential expression $\left(t-\hat{n}\cdot\vec{r}(t)/c\right)$ the position vector is written as $\vec{r}(t)/c=\beta\left(\int_0^t\sin[\vartheta(t')]dt'\;\hat{e_x}+\int_0^t\cos[\vartheta(t')]dt'\;\hat{e_z}\right)$. With the substitution $t'=z'/c$ it follows

$$c\left(t-\hat{n}\cdot\vec{r}(t)/c\right)=\int_0^z\left(1-\beta\cos[\theta]\cos[\vartheta(z')]-\right.$$
$$\left.-\beta\sin[\theta]\sin[\vartheta(z')]\right)dz'. \quad (10)$$

Expansion of the integrand in second order as above results in $1/2\gamma^2\left(1+\gamma^2(\theta-\vartheta)^2\right)$ and in Eq. (6). Also this expansion is very accurate since higher order terms attribute in forth order.

It should be mentioned that in [5] the spectral power density was calculated with an incorrect equation, rendering Fig. 14 and 18 to be obsolete.

References

[1] A. V. Korol, A. V. Solov'yov, W. Greiner, Channeling and Radiation in Periodically Bent Crystals, 2nd edn., Springer Heidelberg, New York, Dordrecht, London, Springer-Verlag Berlin Heidelberg 2014, 2014, Springer Series on Atomic, Optical and Plasma Physics 69, 2014.

[2] A. V. Pavlov, A. V. Korol, V. K. Ivanov, A. V. Solov'yov, Channeling and radiation of electrons and positrons in the diamond heterocrystals, St. Petersburg Polytechnic University Journal. Physics and Mathematics 14 (2021) 190–201. doi:https://doi.org/10.18721/JPM.14414.

[3] J. Lindhard, Influence of Crystal Lattice on Motion of Energetic Charged Particles, Mat. Fys. Medd. Dan. Vid. Selsk. 34 no.14 (1965) 1–64, .

[4] H. Backe, De-channeling in terms of instantaneous transition rates: computer simulations for 855 MeV electrons at (110) planes of diamond, The European Physical Journal D 76 (2022) 153–168. doi:10.1140/epjd/s10053-022-00464-w.

[5] H. Backe, On planar (110) channeling of 500 MeV positrons and electrons in silicon semiconductor detectors, Nuclear Instruments and Methods in Physics Research A 1059 (Nuclear Instruments and Methods in Physics Research A) (2024) 168998, 9th International Conference "Charged & Neutral Particles Channeling Phenomena". doi:http://doi.org/10.1016/j.nima.2023.168998.

[6] H. Backe, D. Krambrich, W. Lauth, K. Andersen, J. L. Hansen, U. I. Uggerhøj, Radiation emission at channeling of electrons in a strained layer $Si_{1-x}Ge_x$ undulator crystal, Nuclear Instruments and Methods in Physics Research B 309 (0) (2013) 37 – 44, The 5th International Conference "Channeling 2012", "Charged and Neutral Particles Channeling Phenomena, September 23-28, 2012, Alghero (Sardinia), Italy. doi:http://dx.doi.org/10.1016/j.nimb.2013.03.047. URL http://www.sciencedirect.com/science/article/pii/S0168583X13003820

[7] D. W. Palmer, The semiconductors-information (2014).
URL https://www.semiconductors.co.uk

[8] J. Jackson, Classical Electrodynamics, John Wiley & Sons, Inc.,New York, Chichester, Weinheim, Brisbane, Singapore, Toronto, John Wiley & Sons, 605 Third Avenue, New York, NY 10158-0012 (212) 850 -6011, 1999, Third Edition.

[9] C. Brau, Free-Electron Lasers, ACADEMIC PRESS, INC. Boston, San Diego, New York, London, Sydney, Tokyo, Toronto, 24-28 Oval Road, London NW1 7DX, 1990, United Kingdom Edition.

[10] H. Backe, W. Lauth, P. Drexler, P. Heil, P. Klag, B. Ledroit, F. Stieler, Design study for a 500 MeV positron beam at the Mainz Microtron MAMI, The European Physical Journal D 76 (2022) 150, 10 pages. doi:doi.org/10.1140/epjd/s10053-022-00465-9.